ResearchGate

See discussions, stats, and author profiles for this publication at: https://www.researchgate.net/publication/26263329

Synthesis and Thermostructural Studies of a CuFe1−xCrxO2 Delafossite Solid Solution with 0 <= x <= 1

ARTICLE *in* INORGANIC CHEMISTRY · JUNE 2009

Impact Factor: 4.76 · DOI: 10.1021/ic900437x · Source: PubMed

CITATIONS
26

READS
43

4 AUTHORS, INCLUDING:

Antoine Barnabé
Paul Sabatier University - Toulouse III
65 PUBLICATIONS **1,162** CITATIONS
SEE PROFILE

Philippe Tailhades
Paul Sabatier University - Toulouse III
159 PUBLICATIONS **1,943** CITATIONS
SEE PROFILE

Available from: Philippe Tailhades
Retrieved on: 31 January 2016

Inorganic Chemistry
Article

Inorg. Chem. **2009**, *48*, 6065–6071 **6065**
DOI: 10.1021/ic900437x

Synthesis and Thermostructural Studies of a $CuFe_{1-x}Cr_xO_2$ Delafossite Solid Solution with $0 \leq x \leq 1$

M. Lalanne, A. Barnabé,* F. Mathieu, and Ph. Tailhades

Université de Toulouse, UPS Institut Carnot CIRIMAT, 118 Route de Narbonne, 31062 Toulouse Cedex 9, France

Received March 5, 2009

In this work, different $CuFe_{1-x}Cr_xO_2$ compositions with $0 \leq x \leq 1$ were prepared by a standard solid-state reaction. These oxides crystallize with the delafossite structure. The phase stability and thermal behavior of the complete $CuFe_{1-x}Cr_xO_2$ solid solution was studied by thermogravimetric analysis and high-temperature X-ray diffraction experiments under an air atmosphere up to 1000 °C. For $x = 0$, $CuFeO_2$ is oxidized into the spinel ($CuFe_2O_4$) and copper monoxide (CuO) phases, whereas for $x = 1$, $CuCrO_2$ is thermally stable. For all of the intermediate compositions ($0 < x < 1$), complex oxidation, reduction, and phase transitions between delafossite and spinel have been observed. chromium tends to stabilize the stoichiometric delafossite phase, while iron favors the delafossite-to-spinel phase transition.

Introduction

AMO_2 delafossite compounds derived from the $CuFeO_2$ mineral are quite interesting materials because of their ability to be stabilized with a large number of A and M cations and within a wide range of off-stoichiometry values, leading to different physical properties.[1,2] In particular, delafossite compounds with M = {Al, Ga} have attracted much attention as p-type transparent conducting oxides (TCOs) in the past decade.[3] Nowadays, studies on delafossite oxides are interesting not only for the TCO properties but also for applications such as in catalysis,[4] magnetics,[5] and possibly thermoelectrics.[6,7]

The delafossite structure can accommodate monovalent noble metal cations $A^+ = \{Cu^+, Ag^+, Pd^+, Pt^+\}$ and trivalent cations M^{3+} with ionic radii varying from 0.535 Å (octahedral Al^{3+} ion) up to 1.032 Å (octahedral La^{3+} ion) according to Shannon's table of effective ionic radii.[8] The AMO_2 delafossite structure can be described as a stacking of MO_2 layers made of edge-sharing MO_6 octahedra that are connected by planes of A^+ cations arranged as a triangular network (Figure 1). Each A^+ cation is linearly coordinated by two O^- anions belonging to the upper and lower MO_2 layers. The oxygen layers can be stacked in different ways along the *c* axis in order to form two polytypes of the delafossite structure: the hexagonal 2H (space group $P6_3/mmc$) and the rhombohedral 3R (space group $R\bar{3}m$) polytypes.

The synthesis[1,9−12] and thermodynamic,[13,14] electric,[15] optoelectric,[16] thermoelectric,[17] lithium intercalation,[18] and magnetic properties[19] of $CuMO_2$ with M = Fe have been intensively studied so far: $CuFeO_2$ delafossite is a well-known p-type semiconductor with an antiferromagnetic behavior

*To whom correspondence should be addressed. E-mail: barnabe@chimie.ups-tlse.fr.

(1) Shannon, R. D.; Rogers, D. B.; Prewitt, C. T. *Inorg. Chem.* **1971**, *10*, 713–718.
(2) Doumerc, J. P.; Ammar, A.; Wichainchai, A.; Pouchard, M.; Hagenmuller, P. *J. Phys. Chem. Solids* **1987**, *48*, 37–43.
(3) Kawazoe, H.; Yasukawa, M.; Hyodo, H.; Kurita, M.; Yanagi, H.; Hosono, H. *Nature* **1997**, *389*, 939–942.
(4) Monnier, J. R.; Apai, G. R.; Hanrahan, M. J. U.S. Patent 4,748,144, **1988**.
(5) El Ataoui, K.; Doumerc, J. P.; Ammar, A.; Grenier, J. C.; Fournès, L.; Wattiaux, A.; Pouchard, M. *Solid State Sci.* **2005**, *7*, 710–717.
(6) Yagi, H.; Seo, W.; Koumoto, K. *Key Eng. Mater.* **2000**, *251*, 180–182.
(7) Isawa, K.; Yaegashi, Y.; Ogota, S.; Nagano, M.; Sudo, S.; Yamada, K.; Yamauchi, H. *Phys. Rev. B* **1998**, *57*, 7950–7954.
(8) Shannon, R. D. *Acta Crystallogr., Sect. A* **1976**, *32*, 751–767.
(9) Zhao, T. R.; Hasegawa, M.; Koike, M.; Takei, H. *J. Cryst. Growth* **1995**, *148*, 189–192.
(10) Sheets, W. C.; Mugnier, E.; Barnabé, A.; Marks, T. J.; Poeppelmeier, K. R. *Chem. Mater.* **2006**, *18*, 7–20.
(11) Mugnier, E.; Barnabé, A.; Tailhades, Ph. *Solid State Ionics* **2006**, *177*, 607–612.
(12) Barnabé, A.; Mugnier, E.; Presmanes, L.; Tailhades, Ph. *Mater. Lett.* **2006**, *60*, 3468–3470.
(13) Zalazinskii, A. G.; Balakirev, V. F.; Chebotaev, N. M.; Chufarov, G. I. *Russ. J. Inorg. Chem.* **1969**, *14*, 326–328.
(14) Gaddala, M. M.; White, J. *J. Br. Ceram. Soc.* **1964**, *63*, 39–62.
(15) Rogers, D. B.; Shannon, R. D.; Prewitt, C. T.; Gillson, J. L. *Inorg. Chem.* **1971**, *10*, 723–727.
(16) Benko, F. A.; Koffyberg, F. P. *J. Phys. Chem. Solids* **1987**, *48*, 431–434.
(17) Hayashi, K.; Nozaki, T.; Kajitani, T. *Jpn. J. Appl. Phys.* **2007**, *46*, 5226–5229.
(18) Sukeshini, A. M.; Kobayashi, H.; Tabuchi, M.; Kageyama, H. *Solid State Ionics* **2000**, *128*, 33–41.
(19) Terada, N.; Mitsuda, S.; Oohara, Y.; Yoshizawa, H.; Takei, H. *J. Magn. Magn. Mater.* **2004**, *272−276*, e997–e998.

© 2009 American Chemical Society
Published on Web 06/03/2009

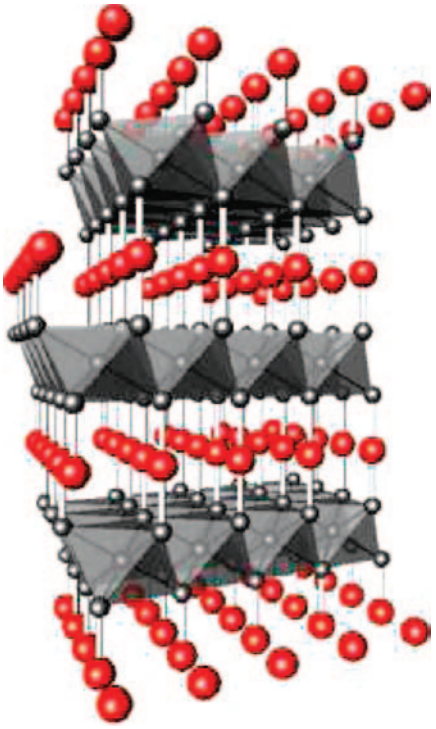

Figure 1. Schematic drawing of the 3R $CuFeO_2$ delafossite structure.

below 13 K and frustrated magnetic interactions in triangular lattices.[20] However, n-type single crystals have also been grown and characterized.[21] The conductivity of p-type $CuFeO_2$ delafossite at room temperature (σ_{RT} = 2 S/cm[15,16]) is the largest among the $CuMO_2$ delafossite series when an off-stoichiometric $CuFeO_{2+\delta}$ delafossite phase is formed. In delafossite compounds, the Cu/M ratio can have an influence on the electrical properties,[22] but the transport properties are mainly governed by the copper mixed valency Cu^{I}/Cu^{II}.[23,24] In $CuFeO_{2+\delta}$, the Cu^{I}/Cu^{II} ratio is directly controlled by the oxygen nonstoichiometry value δ according to $(Cu^{+}_{1-2\delta}Cu^{2+}_{2\delta})Fe^{3+}O_{2+\delta}$. However, for TCO applications, the optical transmittance of $CuFeO_2$ delafossite thin films is limited in the visible region because of its narrow band gap of about 2 eV.

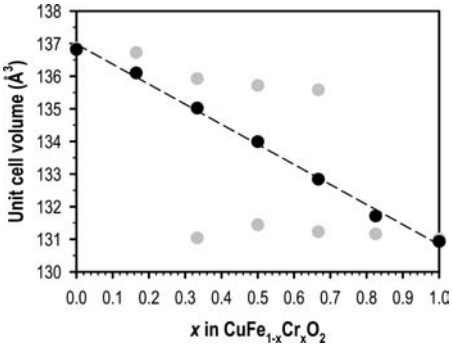

Figure 2. Unit cell volumes of the $CuFe_{1-x}Cr_xO_2$ series with $0 \le x \le 1$ after 10 h of treatment at 900 °C (in gray) and after 30 h at 900 and 1000 °C (in black).

$CuMO_2$ with M = Cr has also been studied for its thermodynamic,[13] magnetic,[25] optoelectronic,[26−30] and thermoelectric [31,32] properties, catalytic activity,[4,33] and lithium insertion:[34] $CuCrO_2$ delafossite is also a p-type semiconductor but with a lower intrinsic electrical conductivity (σ_{RT} = 3.5×10^{-5} S/cm[27]) because of difficulties in inducing an oxygen nonstoichiometric phase in this system. However, $CuCrO_2$ is a more promising TCO than $CuFeO_2$ because of good optical transparency in the visible range with a band gap of about 3.1 eV and with an electrical conductivity that can be drastically improved up to σ_{RT} = 220 S/cm with appropriate doping like in a $CuCr_{0.95}Mg_{0.05}O_2$ thin film.[35] In this case, the copper mixed valency is directly controlled by the doping stoichiometry x according to $(Cu^{+}_{1-x}Cu^{2+}_{x})(Cr^{3+}_{1-x}Mg^{2+}_{x})O_2$.

One can note that the mineral name of $CuCrO_2$ is Mac Connellite. It is worth mentioning that $CuFeO_2$ and $CuCrO_2$ are isostructural compounds. Henceforth, the general term delafossite will be used to refer to the compound studied in this work.

The present study deals with a $CuFe_{1-x}Cr_xO_2$ ($0 \le x \le 1$) solid solution, which can combine the high intrinsic electrical conductivity of $CuFeO_2$ because of its ability to obtain off-stoichiometric compounds and the good optical properties of $CuCrO_2$ in order to obtain new TCO materials. The purpose of this work is to synthesize the complete solid solution $CuFe_{1-x}Cr_xO_2$ with $0 \le x \le 1$ and analyze the effect of oxygen nonstoichiometry on the stability of the delafossite phase using thermostructural analyses.

Experimental Section

Polycrystalline samples of $CuFe_{1-x}Cr_xO_2$ with $0 \le x \le 1$ were prepared by a standard solid-state reaction. Cu_2O, Fe_2O_3, and Cr_2O_3 commercial powders are mixed in stoichiometric quantities. The obtained mixtures have been treated in a nitrogen atmosphere between 900 and 1000 °C for 30 h with intermittent grindings.

Powder X-ray diffraction (XRD) measurements for phase analysis and structural refinement were performed at room temperature using a Bruker AXS D4 diffractometer. Struc-

(20) Mitsuda, S.; Uno, T.; Mase, M.; Nojiri, H.; Takahashi, K.; Motokawa, M.; Arai, M. *J. Phys. Chem. Solids* **1999**, *60*, 1249–1251.
(21) Dordor, P.; Chaminade, J. P.; Wichainchai, A.; Marquestaut, E.; Doumerc, J. P.; Pouchard, M.; Hagenmuller, P.; Ammar, A. *J. Solid State Chem.* **1988**, *75*, 105–112.
(22) Ingram, B. J.; González, G. B.; Mason, T. O.; Shahriari, D. Y.; Barnabé, A.; Ko, D.; Poeppelmeier, K. R. *Chem. Mater.* **2004**, *16*, 5616–5622.
(23) Ingram, B. J.; Mason, T. O.; Asahi, R.; Park, K. T.; Freeman, A. J. *Phys. Rev. B* **2001**, *64*, 155114.
(24) Thomas, G. *Nature* **1997**, *389*, 907–908.
(25) Okuda, T.; Onoe, T.; Beppu, Y.; Terada, N.; Doi, T.; Miyasaka, S.; Tokura, Y. *J. Magn. Magn. Mater.* **2007**, *310*, 890–892.
(26) Benko, F. A.; Koffyberg, F. P. *Mater. Res. Bull.* **1986**, *21*, 753–757.
(27) Nagarajan, R.; Duan, N.; Jayaraj, M. K.; Li, J.; Vanaja, K. A.; Yokochi, A.; Draeseke, A.; Tate, J.; Sleight, A. W. *Int. J. Inorg. Mater.* **2001**, *3*, 265–270.
(28) Tate, J.; Jayaraj, M. K.; Draeseke, A. D.; Ulbrich, T.; Sleight, A. W.; Vanaja, K. A.; Nagarajan, R.; Wager, J. F.; Hoffman, R. L. *Thin Solid Films* **2002**, *411*, 119–124.
(29) Mahapatra, S.; Shivashankar, S. A. *Chem. Vap. Deposition* **2003**, *9*, 238–240.
(30) Li, D.; Fang, X. D.; Deng, Z. H.; Zhou, S.; Tao, R. H.; Dong, W. W.; Wang, T.; Zhao, Y. P.; Meng, G.; Zhu, X. B. *J. Phys. D: Appl. Phys.* **2007**, *40*, 4910–4915.
(31) Okuda, T.; Jufuku, N.; Hidaka, S.; Terada, N. *Phys. Rev. B* **2005**, *72*, 144403.
(32) Ono, Y.; Satoh, K.; Nozaki, T.; Kajitani, T. *Jpn. J. Appl. Phys.* **2007**, *46*, 1071–1075.
(33) Rao, R.; Dandekar, A.; Baker, R. T. K.; Vannice, M. A. *J. Catal.* **1997**, *171*, 406–419.
(34) Shu, J.; Zhu, X.; Yi, T. *Electrochim. Acta* **2008**, in press.
(35) Nagarajan, R.; Draeseke, A. D.; Sleight, A. W.; Tate, J. *J. Appl. Phys.* **2001**, *89*, 8022–8025.

Table 1. Lattice Parameters for a $CuFe_{1-x}Cr_xO_2$ Solid Solution Series with $0 \le x \le 1$

	a (Å)	c (Å)	V (Å^3)
$CuFeO_2$	3.0344(2)	17.158(3)	136.82(2)
$CuFe_{0.835}Cr_{0.165}O_2$	3.0268(2)	17.154(3)	136.10(2)
$CuFe_{0.667}Cr_{0.333}O_2$	3.0159(2)	17.141(2)	135.02(2)
$CuFe_{0.5}Cr_{0.5}O_2$	3.0055(2)	17.128(2)	133.99(2)
$CuFe_{0.333}Cr_{0.667}O_2$	2.9942(2)	17.109(2)	132.84(3)
$CuFe_{0.165}Cr_{0.835}O_2$	2.9826(2)	17.097(2)	131.71(3)
$CuCrO_2$	2.9742(2)	17.090(2)	130.93(2)

tural refinements were made using the Rietveld analysis implemented in the *FullProf-WinPlotR* program. All samples were also analyzed with respect to temperature up to 1000 °C in air using a Bruker AXS D8 diffractometer equipped with a MRI Radiation high-temperature chamber. In all cases, copper radiations were used as the X-ray source ($\lambda_{Cu\ K\alpha_1}$ = 1.5405 Å and $\lambda_{Cu\ K\alpha_2}$ = 1.5445 Å) and filtered with a nickel filter.

The specimens for transmission electron microscopy (TEM) were prepared by crushing polycrystalline powders and mounting the crystal fragments onto a lacey-carbon copper grid. TEM analysis was performed with a Jeol 2100F field emission gun electron microscope operating at 200 kV equipped with a side-entry double-tilt specimen holder. The morphology of the $CuMO_2$ crystals was observed using a Jeol JSM-6400 scanning electron microscope. Energy-dispersive spectroscopy (EDS) was systematically performed on numerous grains.

The specific surface area of the powder was measured using a 70/30 mixture of helium and nitrogen adsorption by the Brunauer−Emmett−Teller (BET) method. The apparatus

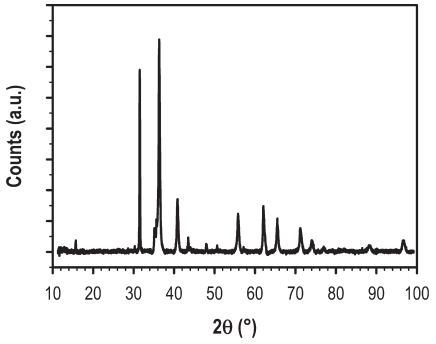

Figure 3. Room temperature XRD pattern of $CuFe_{0.333}Cr_{0.667}O_2$.

Table 2. Specific Surface Areas (S_w) Calculated from BET Measurements and Estimated SEM Particle Sizes for a $CuFe_{1-x}Cr_xO_2$ Solid Solution Series with $0 \le x \le 1$

	S_w (m^2/g)	d_{BET} (μm)	d_{SEM} (μm)
$CuFeO_2$	0.57(2)	1.92(7)	1.6(4)
$CuFe_{0.835}Cr_{0.165}O_2$	1.01(3)	1.08(3)	1.0(3)
$CuFe_{0.667}Cr_{0.333}O_2$	1.36(4)	0.80(2)	0.8(2)
$CuFe_{0.5}Cr_{0.5}O_2$	1.41(4)	0.77(2)	0.7(3)
$CuFe_{0.333}Cr_{0.667}O_2$	1.56(5)	0.69(2)	0.6(2)
$CuFe_{0.165}Cr_{0.835}O_2$	1.75(5)	0.61(2)	0.6(3)
$CuCrO_2$	1.94(6)	0.55(2)	0.5(2)

used was a Micromeritics Flowsorb II 2300 device. The powders were degassed in a nitrogen atmosphere at 250 °C for 30 min to decontaminate the surface before the measurements.

Thermogravimetric analysis (TGA) of samples was recorded with a TAG 1600 Setaram symmetric thermobalance. The samples were heated at 5 °C/min up to 1000 °C in air.

Results and Discussion

$CuFe_{1-x}Cr_xO_2$ Solid Solution. After 30 h of thermal treatment at 900 and 1000 °C under a nitrogen atmosphere with intermittent grindings, all of the synthesized samples of the $CuFe_{1-x}Cr_xO_2$ series with $0 \le x \le 1$ exhibited a single delafossite phase. The complete series of solid solutions $CuFe_{1-x}Cr_xO_2$ with x ranging from 0 to 1 was thus prepared for the first time. For intermediate composition $0 < x < 1$, delafossite phases with lattice parameters in accordance with the iron- and chromium-rich delafossites were obtained after only 10 h of treatment at 900 °C under a nitrogen atmosphere. Longer treatment times and higher temperatures with intermittent grindings were required to obtain a single delafossite solid solution. Variation of the unit cell volume as a result of the thermal treatment is determined from lattice parameter Rietveld refinement as shown in Figure 2. Even though two delafossite phases are present for x = 0.165 and 0.835, they are not represented in Figure 2 because of the weak Bragg peaks in the XRD pattern.

The lattice parameters and unit cell volumes are indicated in Table 1. The XRD pattern for $x = {}^2/_3$ ($CuFe_{0.333}Cr_{0.667}O_2$) is shown in Figure 3. The unit cell parameters are a = 3.0344(2) Å and c = 17.158(3) Å for x = 0 ($CuFeO_2$) and a = 2.9742(2) Å and c = 17.090(2) Å

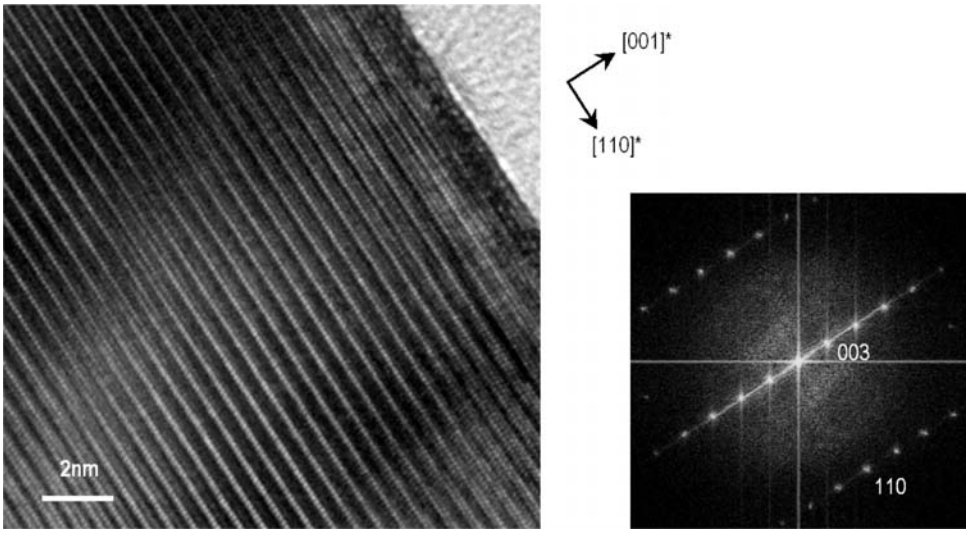

Figure 4. [−110] zone axis HRTEM and corresponding FFT images of the $CuFe_{0.333}Cr_{0.667}O_2$ compound.

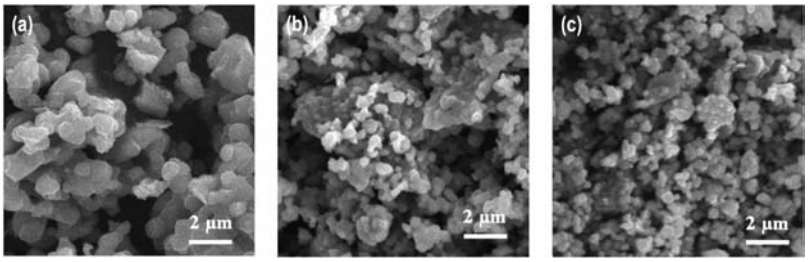

Figure 5. SEM images of the $CuFe_{1-x}Cr_xO_2$ solid solution when x = (a) 0, (b) $^2/_3$, and (c) 1.

for $x = 1$ ($CuCrO_2$). These values are in excellent agreement with those listed in the literature.[1,2,11] The decrease in the unit cell parameters and cell volume with increasing x in $CuFe_{1-x}Cr_xO_2$ well agrees with Vegard's law and with the decrease of the ionic radius as iron with $r(Fe^{3+}_{coord\ VI}) = 0.645$ Å is replaced by chromium with $r(Cr^{3+}_{coord\ VI}) = 0.615$ Å. This change in the unit cell volume (−4.3% from $x = 0$ to 1) is rather anisotropic because it is mainly due to the shrinking of the a parameter (−2% from $x = 0$ to 1), whereas the c parameter remains more or less constant (−0.3% from $x = 0$ to 1). The O−Cu−O bond lengths along the c axis are quite unaffected by the iron-to-chromium substitution, whereas the a parameter decreases proportionally to the edge of the MO_6 octahedral when x increases. This anisotropy induces a constant decrease of the distortion of the MO_6 octahedra from iron to chromium, which can be correlated to the covalence of the metal-to-oxygen bond.[2]

The $x = {}^2/_3$ ($CuFe_{0.333}Cr_{0.667}O_2$) sample has been investigated by TEM. The electron diffraction (ED) pattern has been indexed in the 3R delafossite structure with $a \approx 3.0$ Å and $c \approx 17.1$ Å. As illustrated in Figure 4, corresponding to the [−110] zone axis, a high-resolution transmission electron microscopy (HRTEM) micrograph and the corresponding Fourier function transform (FFT) exhibit well-defined regular stacking along the c axis. No other phase or polytype has been observed. In particular, no iron- or chromium-rich delafossite phase can be detected in the ED patterns and/or EDS measurements. Only occasionally has disorder in the stacking of successive cationic layers been observed in accordance with XRD pattern anisotropic peak broadening.

The nitrogen adsorption of the as-synthesized powders was measured by the BET method. The specific surface areas S_w for all of the $CuFe_{1-x}Cr_xO_2$ ($0 \le x \le 1$) samples are listed in Table 2. The specific surface areas are between 0.5 and 2 m^2/g in accordance with powder synthesis at such high temperature. The larger the value of x, the more the specific surface area continuously increases according to Vegard's law, i.e., from 0.5 m^2/g for $x = 0$ ($CuFeO_2$) to 2 m^2/g for $x = 1$ ($CuCrO_2$). From the BET specific surface areas, the particle diameters d_{BET} were calculated according to the equation $d_{BET} = 6/\rho S_w$ (ρ is the crystallographic density determined from the lattice parameters). For this calculation, it is necessary to assume that the grains are spherical with a monodisperse distribution. d_{BET} continuously decreases from 1.9 μm for $x = 0$ to 0.6 μm for $x = 1$, as indicated in Table 2. These particle size estimations are in agreement with the medium grain size d_{SEM} observed by scanning electron microscopy (SEM) for all of the compositions (Table 2). SEM images for $x = 0$, $^2/_3$, and 1 (Figure 5) are in quite good agreement with the assumption about the spherical shape and the narrow distribution of the particle size distribution of the particles.

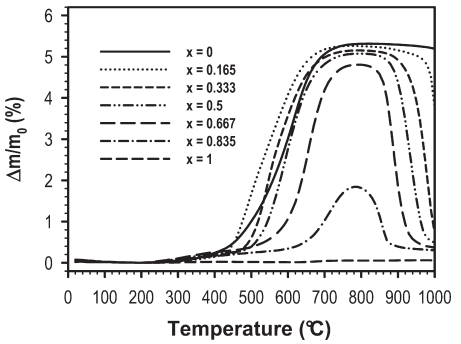

Figure 6. TGA measurements in air for the $CuFe_{1-x}Cr_xO_2$ solid solution series with $0 \le x \le 1$.

$CuFe_{1-x}Cr_xO_2$ Thermostructural Behavior. Significant quantities of oxygen can be quickly and easily intercalated into the $Cu^{1+}M^{3+}O_2$ delafossite only when the M cations exceed a certain size, leading to off-stoichiometric $Cu^{1+}M^{3+}O_{2+\delta}$. This is because O^- anions have enough space to be intercalated between copper atoms in the copper plane. As the M cations become smaller, the Cu−Cu distances become too short for such oxygen passage.[11] Thus, oxygen intercalation into $Cu^{1+}M^{3+}O_2$ delafossite is forced or is even not possible if the M cations are too small.

The phase stability and thermal behavior of the $CuFe_{1-x}Cr_xO_2$ solid solution was studied by TGA and high-temperature XRD under an air atmosphere up to 1000 °C in order to characterize the oxygen intercalation with a decrease in the M^{3+} cation size from iron with $r(Fe^{3+}_{coord\ VI}) = 0.645$ Å to chromium with $r(Cr^{3+}_{coord\ VI}) = 0.615$ Å. TGA curves are plotted in Figure 6.

For $x = 0$, i.e., for $CuFeO_2$, the TGA experiment shows two weight gains. A slight oxidation of cuprous ions appears, leading oxygen intercalation from about 400 to 500 °C. An off-stoichiometric $CuFeO_{2+\delta}$ delafossite phase is then formed.[11] Above 500 °C, a phase transition occurs, leading to copper monoxide (CuO) and cuprospinel ($Cu_xFe_{3-x}O_4$) phases. Quantitative XRD analysis indicates that the copper content is equally distributed between the CuO and cuprospinel phases. It can then be deduced that the composition of the cuprospinel phase is $x = 1$ ($CuFe_2O_4$) in accordance with the thermodynamic phase diagram.[13,14] XRD experiments at high temperature confirm this phase transition (Figure 7a). For $M^{3+} = Fe^{3+}$, oxygen intercalation is possible but is limited to low δ values. Although the

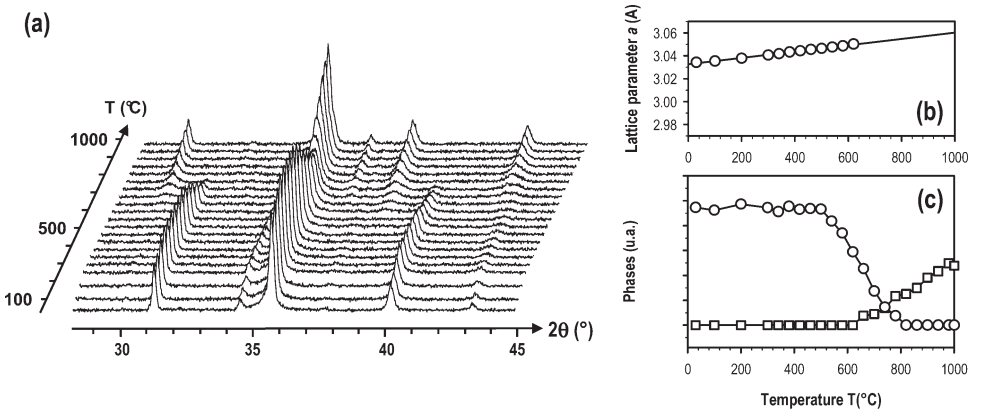

Figure 7. (a) Change in the XRD patterns of $CuFeO_2$ with respect to temperature (b). Corresponding change in the *a* lattice parameter with respect to the temperature. (c) Relative change in the phase intensities of delafossite (circle) and spinel (square).

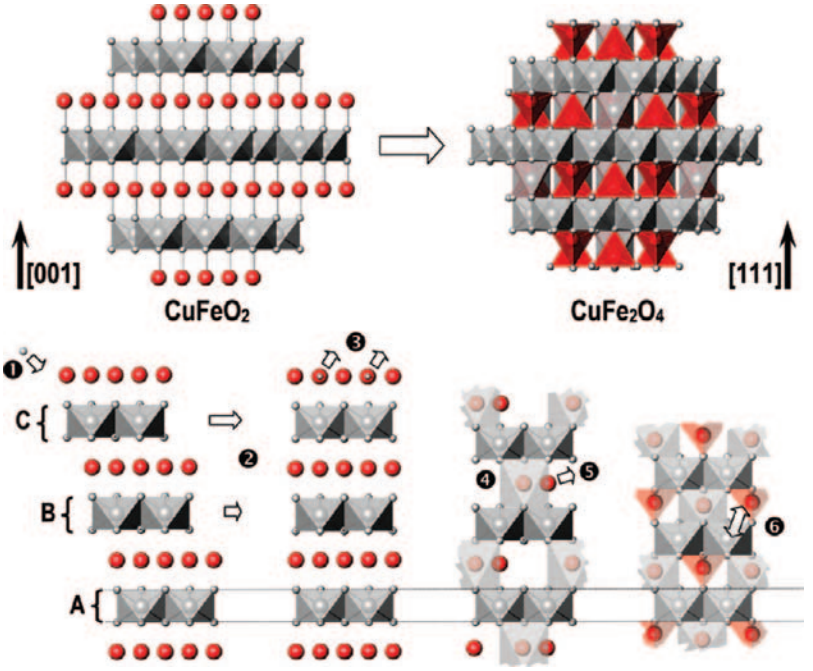

Figure 8. Schematic representation of the structural mechanism for the delafossite-to-spinel phase transition.

radius of the ferric iron ions [$r(Fe^{3+}) = 0.645$ Å] is below the theoretical critical radius, allowing oxygen intercalation ($r_c = 0.70$ Å)[11] at room temperature, off-stoichiometric $CuFeO_{2+\delta}$ can be obtained at intermediate temperature because of the unit cell dilation. Figure 7b represents the linear variation of 0.003% per degree Celsius of the *a* parameter with temperature, as soon as it can be measured properly. For example, the *a* parameter is equal to 3.05 Å at $T = 550$ °C, which is 0.5% higher than the room temperature value. With a quite constant variation along the *c* axis (less than 0.1%), this leads to a volumic variation of 1.2% in the same temperature range. Even if additional space for oxygen intercalation becomes available at elevated temperature, off-stoichiometric delafossite intercalation is forced. This induces defects in the Cu−Cu plane first before leading to the delafossite-to-spinel phase transition. This is confirmed by the continuous decrease in the intensity and the heterogeneous enlargement of the Bragg peaks belonging to the delafossite phases during oxidation, followed by the apparition of the characteristic peaks belonging to the spinel and CuO phases. Quantification of the relative change of the main crystallographic phases is done at all temperatures by measuring the intensity of two isolated characteristic Bragg peaks [(006) at 31.5° in 2θ for delafossite and (220) at 30° in 2θ for spinel]. The values for the delafossite and spinel phases for $x = 0$ are reported in Figure 7c.

By analogy to a previous work on the structural analysis of the transformation mechanisms in iron oxides,[36] a detailed structural mechanism is proposed to explain this delafossite-to-spinel phase transition. This mechanism is schematically illustrated in Figure 8, and the main steps are labeled from 1 to 6. The delafossite structure ($R\bar{3}m$) is a compact stacking of O^- anions of the ABC type along the *c* axis. The first layer of the FeO_6 octahedra is the reference of the structural mechanism; it will then be assumed to be static in our model. The intercalation of extra oxygen atoms within the copper layers (step 1) induces a shearing of the [FeO_2] layers. The

(36) Mathieu, F.; Rousset, A. *Philos. Mag. A* **1993**, *67*, 533–555.

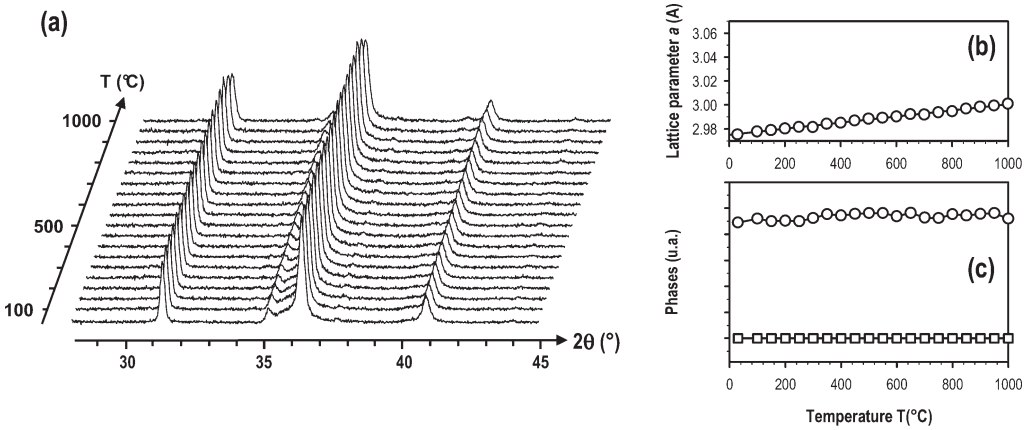

Figure 9. (a) Change in the XRD patterns of $CuCrO_2$ with respect to temperature. (b) Corresponding change in the *a* lattice parameter with respect to the temperature. (c) Relative change in the phase intensities of delafossite (circle) and spinel (square).

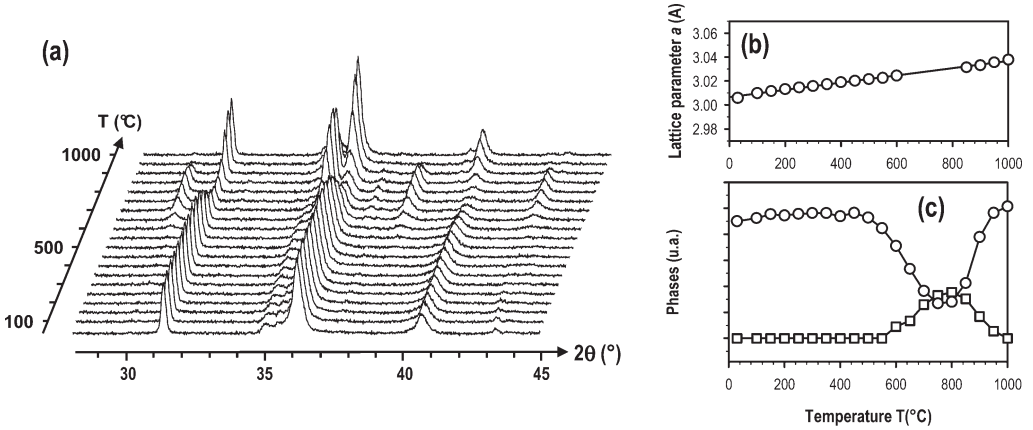

Figure 10. (a) Change in the XRD patterns of $CuFe_{0.333}Cr_{0.667}O_2$ with respect to temperature. (b) Corresponding change in the *a* lattice parameter with respect to the temperature. (c) Relative change in the phase intensities of delafossite (circle) and spinel (square).

second and third layers are then moved along the Burgers vectors $t = \left[\frac{2}{3}\frac{1}{3}0\right]$ and $\left[\frac{4}{3}\frac{2}{3}0\right]$, respectively, with respect to the first layer (step 2). Half of the total copper atoms and their corresponding extra oxygen atoms get out of the structure and are simultaneously oxidized into CuO (step 3). A quarter of the total copper atoms stay in their environment, which is becoming an octahedral sublattice (step 4). The last quarter of the total copper atoms diffuse between the $[FeO_2]$ layers to be stabilized in the tetrahedral sites (step 5). Because of the relative stabilities of the Fe^{3+} and Cu^{2+} species in the octahedral and tetrahedral sites of the spinel structure,[37] Cu^{2+} ions diffuse into the FeO_6 octahedral layer, replacing the Fe^{3+} cations, which themselves diffuse to the tetrahedral sites located between the two lower oxygen layers. Finally, Fe^{3+} cations diffuse from the first FeO_6 octahedral layer to the tetrahedral sites into the two first oxygen layers (step 6). This is the same as the cationic diffusion into the second and third octahedral layers.

For $x = 1$, i.e., $CuCrO_2$, no weight gain and no phase transition have been observed up to 1000 °C in air. $CuCrO_2$ is thermally stable in air up to 1000 °C.[38] The Rietveld analysis of high-temperature XRD measurements shows that $CuCrO_2$ and $CuFeO_2$ exhibit the same linear variation of the *a* parameter of 0.003% per degree Celsius (see Figure 9). For $CuCrO_2$, the cell parameter *a* is then never high enough to intercalate O^- anions ($a_{max} = 3.00$ Å), i.e., to allow cuprous ion oxidation.

For all of the intermediate compositions of $CuFe_{1-x}Cr_xO_2$ where $0 < x < 1$, complex redox reactions and phase transitions in both delafossite and spinel have been observed with TGA measurements (Figure 6). First, from about 500 to 700 °C, the TGA measurements show a weight gain for $CuFe_{1-x}Cr_xO_2$ compounds corresponding to the oxidation of cuprous ions. Simultaneously, we observed by high-temperature XRD that the delafossite phase is transformed into spinel and CuO phases. Nevertheless, as the chromium content shifts to higher values, the oxidation and phase-transition temperatures increase. This can be explained by variation of the M^{3+} cation size. The substitution of iron by chromium leads to a decrease in the average M^{3+} radius, $r(M^{3+})$. The oxygen intercalation then becomes more difficult and requires higher temperatures to sufficiently dilate the delafossite structure to allow oxygen insertion.

The as-formed spinel and CuO phases are then reduced to delafossite above approximately 800 °C. TGA measurements show a weight loss of about 5% corresponding to the reduction of all Cu^{II} ions to Cu^{I} ions. This reduction is systematically correlated to a phase transition from spinel and monoxide to delafossite as a reverse option of the first phase transition. Figure 10 shows the thermodiffractograms of a sample with $x = {}^2/_3$ ($CuFe_{0.333}Cr_{0.667}O_2$), which

(37) Navrotsky, A.; Kleppa, O. J. *J. Inorg. Nucl. Chem.* **1967**, *29*, 2701–2714.
(38) Saadi, S.; Bouguelia, A.; Trari, M. *Sol. Energy* **2006**, *80*, 272–280.

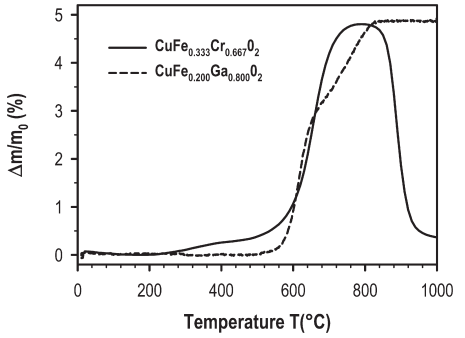

Figure 11. Comparative TGA measurements in air for $CuFe_{0.2}Ga_{0.8}O_2$ and $CuFe_{0.333}Cr_{0.667}O_2$.

is subjected to such reversible redox reaction phenomena and related phase transformations.

In the case of $M^{3+} = Fe^{3+}$, the $CuFe_2O_4$ spinel phase is only transformed into the $CuFeO_2$ phase after annealing at 1050 °C. From the thermodynamic data, one sees that the reduction of Cu^{2+} into Cu^{+} occurs above 1000 °C in air.[39] Indeed, the TGA curve of $CuFeO_2$ (Figure 6) shows a slight weight loss at 1000 °C. For $0 < x < 1$ as well as for increased chromium quantities, the reduction temperature is lowered. This means that chromium facilitates the reduction of the spinel and CuO phases. The thermodynamic data of Navrotsky and Kleppa[37] and the structural description of the delafossite and spinel phases can explain this behavior: when $x > 0$, the delafossite-to-spinel phase transition occurs mainly with the same structural mechanism as that described for $x = 0$. By contrast, however, Cr^{3+} ions are more stable than Cu^{2+} ions in an octahedral environment. In this case, the Cr^{3+} and Cu^{2+} cations do not diffuse into the pure octahedral and mixed tetrahedral/octahedral layers in the spinel structure, keeping the stacking sequence almost unchanged. The delafossite structure becomes more stable than the spinel structure as soon as chromium is substituted for iron. Thus, chromium ions tend to stabilize the stoichiometric delafossite phase, whereas ferric ions make cuprous ion oxidation possible and favor the delafossite-to-spinel phase transition.

Three successive thermal treatments of the sample with $x = {}^2/_3$ ($CuFe_{0.333}Cr_{0.667}O_2$) under an air atmosphere at 1000 °C lead to three successive oxidations and reductions always associated with delafossite-to-spinel and spinel-to-delafossite phase transitions, clearly showing the reversibility of the process.

$CuFe_{0.2}Ga_{0.8}O_2$ delafossite was prepared in order to compare the effect of preferential coordination of M^{3+} to the stability of the delafossite structure. In fact, this mixed gallium/iron delafossite is very interesting because the calculated mean radius of M^{3+} ions in this phase is close to 0.625 Å, the value previously determined for $CuFe_{0.333}Cr_{0.667}O_2$ according to Shannon's table of ionic radii.[8] The stability difference between $CuFe_{0.2}Ga_{0.8}O_2$ and $CuFe_{0.333}Cr_{0.667}O_2$ is then only due to the coordination preference of gallium and chromium cations for octahedral or tetrahedral sites because no significant interference from the dimensional effect is present in this case.

$CuFe_{0.2}Ga_{0.8}O_2$ exhibits a single delafossite phase with lattice parameters similar to those of $CuFe_{0.333}Cr_{0.667}O_2$, according to what was expected from the calculated mean M^{3+} radii. Figure 11 shows that both delafossites are oxidized in the same temperature range. CuO and spinel oxide are precipitated for both gallium- and chromium-containing samples when the weight gain becomes higher than about 4.5%. At higher temperature (from about 900 to 1000 °C), however, the delafossite structure is formed again for the chromium-containing sample but not for the gallium-containing one. For the chromium-containing spinel, because of very strong stabilization of the chromium ions in the octahedral sites,[37] the copper ions are mainly located in the tetrahedral sites of the spinel structure. In other words, the mechanism previously described for $CuFeO_2$ in Figure 8 stops at step 5, i.e., before diffusion of the cationic species between the pure octahedral layers. For the gallium-containing spinel, because of stabilization of the gallium ions in the tetrahedral sites, the copper ions are mostly located in the pure octahedral layers. This corresponds to step 6 already described for the iron-containing samples. The reduction of cupric ions to cuprous ions is probably easier when they are located in tetrahedral sites because tetrahedral cuprous ions are more difficult to oxidize than octahedral cuprous ions.[40] Consequently, the cupric ion reduction would be easier for the chromium-containing sample. The migration of cuprous ions in 2-fold-coordinated sites would then be enough to induce the formation of the delafossite structure. For the gallium sample, more energetic activation would be required.

Conclusion

The complete $CuFe_{1-x}Cr_xO_2$ ($0 \le x \le 1$) delafossite solid solution has been prepared by solid-state reaction at high temperature in an inert atmosphere. According to Vegard's law and a decrease of the ionic radius from $r(Fe^{3+}_{\text{coord VI}})$ to $r(Cr^{3+}_{\text{coord VI}})$, the unit cell parameters and cell volume decrease as x in $CuFe_{1-x}Cr_xO_2$ increases. A thermostructural study has revealed that, with heating in air up to 1000 °C, the $CuFe_{1-x}Cr_xO_2$ ($0 \le x \le 1$) compounds of the solid solution are oxidized into spinel and CuO phases, except for $CuCrO_2$, which is stable in this range of temperature. Chromium ions make it difficult for the oxidation and phase transition to proceed. Temperature-dependent XRD experiments have also shown that delafossite cell parameters vary linearly up to the phase transition into spinel and CuO phases. At high temperatures, the spinel and CuO phases can be reduced back to delafossite when the chromium quantity is enough. A structural mechanism has been proposed to explain this delafossite-to-spinel transition. For $x = 0$, the spinel structure is stable and the phase transition is not reversible. For $x > 0$, the substitution of Fe^{3+} by Cr^{3+} makes the formation of the delafossite phase easier. Preferential coordination of M^{3+} to the tetrahedral site aids in the stabilization of the delafossite structure, as is confirmed by cationic substitution with gallium. It is noted that the Cu^{2+} cations migrate in the delafossite structure very readily.[41] Half of the total copper ions in the delafossite gets out of the structure in order to oxidize into CuO and, subsequently, the copper ions in CuO reenter the delafossite structure during the spinel-to-delafossite transition.

(39) Kenfack, F.; Langbein, H. *Cryst. Res. Technol.* **2004**, *39*, 1070–1079.

(40) Kester, E.; Gillot, B.; Perriat, P.; Dufour, Ph.; Villette, C.; Tailhades, Ph.; Rousset, A. *J. Solid State Chem.* **1996**, *126*, 7–14.

(41) Mugnier, E.; Pasquet, I.; Barnabé, A.; Presmanes, L.; Bonningue, C.; Tailhades, Ph. *Thin Solid Films* **2005**, *493*, 49–53.